Pre-Clinical Research Report

Journal of INTERNATIONAL MEDICAL RESEARCH

Journal of International Medical Research
2025, Vol. 53(5) 1–15

DOI: 10.1177/03000605251340338
journals.sagepub.com/home/imr
Sage

The therapeutic potential of irisin in alleviating acute lung injury via inflammation and ferroptosis modulation

Feng Zhang[1], Jiangpeng Wang[2], Wei Wang[2], Gang Chen[3], Huan Tang[2] and Xuezhen Zhai[4]

Abstract

Objective: Acute lung injury is a fatal complication triggered by sepsis, characterized by widespread inflammation and weakening of the alveolar epithelium. Irisin has been reported to exert anti-inflammatory effects, which are produced by the cleavage of fibronectin type III domain-containing protein 5 in skeletal muscle. Here, we investigated the potential of irisin in preventing acute lung injury by protecting the alveolar epithelium.

Methods: The sepsis-related acute lung injury model was established by a cecal ligation and puncture model in C57/BL6N mice. Lung histology was assessed using hematoxylin and eosin and Masson staining. Ferroptosis-related proteins and genes were quantified via western blot and quantitative polymerase chain reaction, respectively, whereas cytokine levels were measured using enzyme-linked immunosorbent assay.

Results: Histological analysis revealed lung injury in the cecal ligation and puncture group, alongside elevated levels of cytokines such as IL-1β, IL-18, and TNF-α compared with controls. Treatment with irisin mitigated sepsis-induced lung damage and reduced oxidative stress, as indicated by reactive oxygen species and Fe^{2+} levels. Furthermore, irisin pretreatment inhibited the upregulation of ferroptosis-related genes (*Acsl4*, *Ptgs2*, and *Hspa5*) as well as ACSL4, COX-2, and p-AMPK expression.

Conclusion: These findings suggest that irisin treatment is associated with reduced ferroptosis and inflammation in sepsis-induced acute lung injury. Irisin emerges as a promising candidate for acute lung injury therapy induced by sepsis.

[1]Department of Pediatrics, Huaiyin Maternal and Child Health Hospital, China
[2]Department of Cardiovascular Medicine, Huai'an Fifth People's Hospital, China
[3]Department of Respiratory Medicine, Huai'an Fifth People's Hospital, China
[4]Department of Infectious Diseases, Huai'an Fifth People's Hospital, Huai'an, China

Corresponding author:
Xuezhen Zhai, Department of Infectious Diseases, Huai'an Fifth People's Hospital, Changjiang Road, Huai'an, China.
Email: xuezhenzhai86@gmail.com

Keywords
Ferroptosis, irisin, inflammation, lung injury, sepsis

Date received: 21 November 2024; accepted: 17 April 2025

Introduction

Sepsis is a fatal condition represented by uncontrolled response to pathogens. This widespread inflammation may damage body organs, with cases of acute lung injury (ALI) often reported in sepsis.[1] ALI can progress to acute respiratory distress syndrome (ARDS), which has high mortality rates with no effective treatments.[2] Multiple factors lie in the causal pathway of sepsis-related ARDS.[3] It is postulated that ALI/ARDS is induced by inflammatory cytokines which lead to damage to the lung microvascular barrier.[4] Septic ALI is greatly influenced by severe acute inflammation.[5] Pathogens trigger a chain of reactions involving neutrophils and monocytes which migrate to the injury area. In addition, the body releases inflammatory molecules (TNF-α, IL-1β, and IL-6). This damages the alveolar–capillary barrier and makes them leaky, leading to ALI as a complication of sepsis.[6]

Ferroptosis has been shown to enhance sepsis development. Pathogenically, ferroptosis is marked by a buildup of iron and products of membrane lipid peroxidation, followed by cell death. Currently, studies investigating the pathogenesis of ferroptosis mainly focus on iron metabolism and oxidative damage.[7] Drugs that inhibit ferroptosis may help reduce inflammation and protect organs in the context of sepsis, potentially leading to better survival rates.[8] *In vitro* experiments showed that SLC7A11 and Gpx4 (ferroptosis indicators) were decreased in ALI.[9] On the contrary, the concentration of total iron and malondialdehyde (MDA) decreased following lipopolysaccharide (LPS) administration in mice.[9] Ferrostatin-1, a specific blocker of ferroptosis, may abolish the aforementioned effects.[9] Against this background, ferroptosis may facilitate the occurrence of LPS-induced ALI.

Irisin was first discovered in mouse skeletal muscle in 2012.[10] It is a polypeptide formed by the hydrolysis of fibronectin type III domain-containing protein 5 (FNDC5), primarily derived from skeletal muscle and adipose tissue.[11] Following its release from FNDC5, irisin increases the expression of mitochondrial uncoupling protein 1 (UCP 1), which converts white adipose tissue into beige adipose tissue.[12] The presence of irisin in various tissues indicates its involvement in multiple disease progression, including inflammation, metabolic diseases, neurogenesis, and aging.[13] Recently, several studies on humans and animals have demonstrated that irisin reduces obesity-associated pathological effects such as vascular inflammation.[14,15] Irisin has been reported to reduce inflammation in several organs.[16–20] In addition, irisin also suppresses ferroptosis in lung ischemia/reperfusion injury.[21] Notably, irisin could inhibit reactive oxygen species (ROS) generation and inhibit oxidative damage in lung ischemia/reperfusion injury.[21,22] Furthermore, irisin was reported to exert antioxidant activity and suppress oxidative damage in gestational diabetes.[23] In this study, we explored if irisin could ameliorate lungs from sepsis-induced injury and explored its connection to ferroptosis. The goal was to identify new approaches to treating lung complications of sepsis.

Methods

Ethical approval

The study was approved by the Animal Ethics Review Committee of Huai'an Fifth People's Hospital (HF209823). The research related to animal use has complied with the national regulations and institutional policies for the care and use of animals and followed the Animal Research: Reporting of In Vivo Experiments (ARRIVE) guidelines.[24]

Animals

C57/BL6N male mice (8–10 weeks old, weighing 22–25 g) were housed in specific pathogen-free animal rooms with adequate ventilation, lighting, clean cages, a constant relative humidity of 50%–60%, and an appropriate room temperature. All mice had free access to food and water, and their bedding was changed frequently.

Construction of mice model of ALI

The cecal ligation and puncture (CLP) model was selected because it closely replicates polymicrobial sepsis observed in clinical settings. Unlike LPS-induced endotoxemia, CLP induces a dynamic septic response, leading to multiorgan dysfunction, including ALI. This model is widely accepted for studying sepsis pathophysiology and therapeutic interventions. The animals were randomly assigned into three groups: sham group (n = 6), CLP group (n = 6), and CLP + irisin group (n = 6). The CLP model was established as previously described.[25] Briefly, a 1 cm abdominal incision left to midline was performed under 3% isoflurane anesthesia. Subsequently, 60% of the cecum was ligated, and the cecum was punctured twice using a 22-gauge needle to induce mild-grade sepsis. Buprenorphin (0.05 mg/kg) was administrated to mice postoperation for analgesia every 12 h for the first 2 days after procedure. The administrated dose of irisin was referenced according to the previous study by Han et al.[26] Mice received daily irisin (MCE, HY-P72534) treatment via intravenous injection (0.5 mg/kg body weight) starting after the CLP procedure for 3 days.[26] After the final irisin dose, the mice were euthanized in a humane manner via cervical dislocation. Animal death was confirmed by the absence of a heartbeat, respiratory movement, and corneal reflex. Lungs and blood samples were then collected for further analysis; approximately 200 μL blood samples were collected from the ventricle of the heart immediately after euthanasia.

Single-cell sequencing data acquisition, preprocessing, and visualization

We obtained publicly available single-cell RNA-sequencing (scRNA-seq) data from the Gene Expression Omnibus (GEO) database under accession number GSE207651.[27] Raw count matrices (or processed count data) and associated metadata were downloaded for the sham, CLP, and CLP-48h groups. Raw count matrices were loaded and processed using the Seurat package (v4.1.1; Satija Lab, New York Genome Center, NY, USA) in R (v4.1.3; R Core Team, R Foundation for Statistical Computing, Vienna, Austria). All samples were corrected for batch effects and integrated using the reciprocal principal component analysis (RPCA) method, followed by normalization using the LogNormalization method. For each specimen, genes expressed in <3 cell were discarded. Cells with <200 or >10,000 genes; cells with >10% unique molecular identifiers (UMIs) mapped to mitochondrial genes; and cells with >10% UMIs mapped to erythrocyte genes were discarded. For normalization, UMI counts for all nuclei were scaled by library size (total UMI counts), multiplied by 10,000 and transformed to a log scale. Highly variable genes were identified

using the function FindVariableFeatures in Seurat. The top principal components, determined by the PCElbowPlot function, were selected for dimensionality reduction, clustering with resolution = 0.9 and visualization with t-distributed stochastic neighbor embedding (t-SNE).

Marker gene identification and cell-type annotation

Marker genes for each cluster were identified with a Bimod test implemented in the FindAllMarkers function with the following criteria: adjusted p-value < 0.01 (controlled for false discovery rate), only.pos = true, log fold change ≥ 0.25, and genes detected in $< 10\%$ of the cells within their corresponding cluster were excluded. All specimens were normalized using the sctransform method and integrated using the RPCA method in IntegrateData. For both integrated datasets, the top 2000 highly variable genes and the first 30 principal components were used for cell alignment before clustering and t-SNE visualization. Genes with a log2 average expression difference 0.585 and $p < 0.05$ were identified as marker genes. In addition, cell-type annotation was performed using SingleR (Dvir Aran Lab, Stanford University, Stanford, CA, USA).

Hematoxylin and eosin staining

The lung tissues were collected and immediately placed in a solution of 10% neutral-buffered formalin for 24 h to preserve the tissue structure. Next, the tissues were processed through a series of treatments of increasing concentrations of ethanol (50%, 70%, and 90%) to dehydrate them. This was followed by treatment with xylene to make them transparent. Finally, the tissues were embedded in paraffin wax and sectioned into slices (5 μm) with a microtome. The sections were placed on glass slides and stained for analysis. Hematoxylin was then applied to stain cell nuclei for 5 min, followed by rinsing three times with running tap water. Eosin reagent was then applied to stain the cytoplasmic components for 3 min. Following staining, the tissue slices were dehydrated in increasing concentrations of alcohol (ethanol) to remove the staining solution. They were treated with xylene to make them transparent. Finally, the sections were attached to glass slides using xylene-based mountant and coverslipped. A light microscope was used to examine the morphology of lung tissue. The alveolar wall thickness was measured and quantified using ImageJ software.

Histoscore

Histopathological changes were assessed using a semiquantitative lung injury scoring system, calculated as described in previous studies.[28] The scoring system evaluated four key pathological features associated with sepsis-induced lung injury: (a) immune cell infiltration severity (0–4), (b) hyaline membrane formation (0 or 1), (c) pulmonary edema (0 or 1), and (d) alveolar septal thickening (0–3). Cell infiltration severity was graded as 0 (normal), 1 (mild), 2 (moderate), 3 (severe), and 4 (highly severe). For each lung sample, a total of 10 randomly selected microscopic fields were analyzed. The final lung injury score was calculated as the sum of these criteria, with higher scores indicating more severe injury. Histological evaluation was performed to quantify inflammatory infiltration using a previously described scoring system.[29] In brief, lung inflammation severity was graded as follows: 0 = no inflammation; 1 = occasional cuffing with inflammatory cells; 2 = most bronchi or vessels surrounded by a thin layer (1–5 cells) of inflammatory cells; and 3 = most bronchi or vessels surrounded by a thick layer (>5 cells) of inflammatory cells. Scoring was

performed in a blinded manner by two independent investigators to minimize bias and improve reproducibility.

Masson's trichrome staining

Excised lung tissues were sectioned, deparaffinized, and rehydrated. They were then rinsed with distilled water and preheated in Bouin's fluid for 1 h at 56°C–60°C or left overnight at room temperature. This was followed by staining with Weigert's iron hematoxylin solution for 10 min for nuclei staining. Subsequently, they were subjected to a 10-min wash on running warm tap water and then stained with Biebrich scarlet-acid fuchsin solution for 10–15 min for muscle fibers staining. Following rinsing with distilled water, the sections were immersed in a phosphomolybdic–phosphotungstic acid solution for 10–15 min. The slides were observed to monitor color changes and subsequently immersed in aniline blue solution for 5–10 min to induce blue staining of collagen fibers. After another round of rinsing with distilled water, the sections were submerged in a 1% acetic acid solution for 2–5 min, followed by another distilled water wash. Dehydration was achieved through treatment with 95% and then absolute ethanol. Finally, the sections were clarified in xylene, dehydrated further, and mounted using a mounting medium. The trichrome-stained slides were then examined using an optical microscope.

Polymerase chain reaction

RNA was isolated from lung tissue using the RNAiso Plus kit (TaKaRa, Dalian, China) following the manufacturer's instructions. The extracted RNA was then reverse-transcribed into cDNA using the HiScript III RT SuperMix for quantitative polymerase chain reaction (qPCR) (Vazyme, Nanjing, China). Quantitative real-time PCR was performed using the ChamQ SYBR qPCR Master Mix (Vazyme) on a StepOnePlus Real-Time PCR System (Applied Biosystems, Foster City, California, USA). Each sample was analyzed in duplicate, and gene expression was calculated using the comparative CT ($2^{-\Delta\Delta CT}$), with GAPDH as the internal control. The primers for *Acsl4* (Forward: 5′-GTGTAGCACTGAACCTGGGAAAG-3′, Reverse: 5′-GCAACAGCAAGCAGACCATAAA-3′), *Ptgs2* (Forward: 5′-GAGTGGTAGCCAGCAAAGCC-3′, Reverse: 5′-GCCAGCACAAAACCAGGATC-3′), *Hspa5* (GRP78) (Forward: 5′-ACGGCTTCCGATAATCAGCC-3′, Reverse: 5′-TCAATCTGGGGAACTCCACG-3′), and *Gaphd* (Forward: 5′-AAGAAGGTGGTGAAGCAGG-3′, Reverse: 5′-GAAGGTGGAAGAGTGGGAGT-3′) were purchased from Sangon Biotech (Shanghai, China).

Enzyme-linked immunosorbent assay (ELISA)

The content of inflammatory factors was determined by ELISA. Each lung homogenate sample was tested in duplicate wells following the manufacturer's guidelines. Briefly, the sample lysates were incubated with the irisin (EM1901, Finetest, Wuhan, China) and IL-1β (H002-1-2), IL-18 (H015-1-2), IL-6 (H007-1-2), and TNF-α (H052-1-2) antibodies provided in the ELISA kit (Nanjing Jiancheng Bioengineering Institute, Nanjing, China) in line with the manufacturer's protocols. After incubation, the cell wells were rinsed to remove unbound substances. A horseradish peroxidase (HRP)-conjugated secondary antibody was added to each well. The reaction was developed using a tetramethylbenzidine substrate, which turns blue in the presence of HRP and changes to yellow upon the addition of the stop solution. A special plate reader was used to read the absorbance at a wavelength of 450 nm.

Glutathione, MDA, and Fe^{2+} assay

The levels of several indicators of cell damage and stress in the lung tissue lysates were measured. These indicators included Fe^{2+} levels, glutathione (GSH), and MDA. The assays were conducted using corresponding commercial assay kits from Sigma-Aldrich (St. Louis, Missouri, USA).

Western blot

A lysis buffer comprising 0.75% SDS, 0.01% bromophenol blue, 0.5% glycerol, and 50 mM Tris, pH 6.8 was used to prepare to extract proteins from lung tissue. The extracted proteins were separated by 10% gel electrophoresis and then transferred to a nitrocellulose membrane. This was followed by blocking of nonspecific binding with 5% milk in Tris-buffered saline for 60 min at room temperature. Subsequently, the membranes were incubated with rabbit anti-AMPK (MCE, Cat# HY-P80541), anti-p-AMPK (MCE, HY-P80452), GPX4 (MCE, HY-P80450), ACSL4 (Santa Cruz Biotechnology, Dallas, Texas, USA; Cat# sc-365230), COX-2 (Abcam, Cambridge, United Kingdom; Cat# ab283574), and GAPDH (MCE, HY-P80137) antibodies at 4°C overnight. They were then incubated with HRP-conjugated secondary antibody (MCE, HY-P8001) at room temperature for 1 h and then imaged with ChemiDoc™ Touch Imaging System (Bio-Rad, Hercules, California, USA) and analyzed with Image Lab (Bio-Rad).

Statistical analysis

Data were processed using GraphPad Prism software (GraphPad Software, San Diego, CA, USA) and expressed as the mean ± SEM. The data distribution was assessed using the Shapiro-Wilk test, confirming that the data are normally distributed. Multiple groups were compared by one-way analysis of variance (ANOVA) with Tukey's post-hoc test. Statistical analysis of histological scores was performed using the Kruskal–Wallis test followed by Dunn's post-hoc test. Statistical differences were considered significant at $p < 0.05$.

Results

Irisin attenuates lung injury in sepsis-induced ALI

We examined plasma irisin levels after CLP and found a significant reduction compared with control mice (Figure 1(b)). The histological examination of lung tissue from mice subjected to CLP exhibited evidence of lung injury. The most significant adverse change was the occurrence of pulmonary edema, increased alveolar wall thickness, and immune infiltration in the CLP-induced mice (Figure 1(a) and (e)). When lung sections were stained with Masson trichrome to identify collagen deposition (depicted in blue in Figure 1(a) and (f)), a noticeably higher accumulation of collagen was observed in the alveolar spaces and around vascular vessels or bronchioles in the CLP group as compared with both the control and CLP + irisin groups. The lung injury scores revealed a significant reduction in the CLP + irisin group compared with the CLP group, suggesting that irisin effectively mitigated the pathological changes in lung tissue (Figure 1(c)). Lung tissues from the CLP group exhibited significantly increased inflammatory cell infiltration compared with controls ($p < 0.05$), characterized by marked neutrophil accumulation around bronchi and blood vessels (inflammation scores: CLP group vs control, $p < 0.05$). However, treatment with irisin significantly decreased inflammatory cell infiltration in lung tissues ($p < 0.05$), demonstrating its potent anti-inflammatory effects in ALI (Figure 1(d)). Overall, these findings indicate that irisin

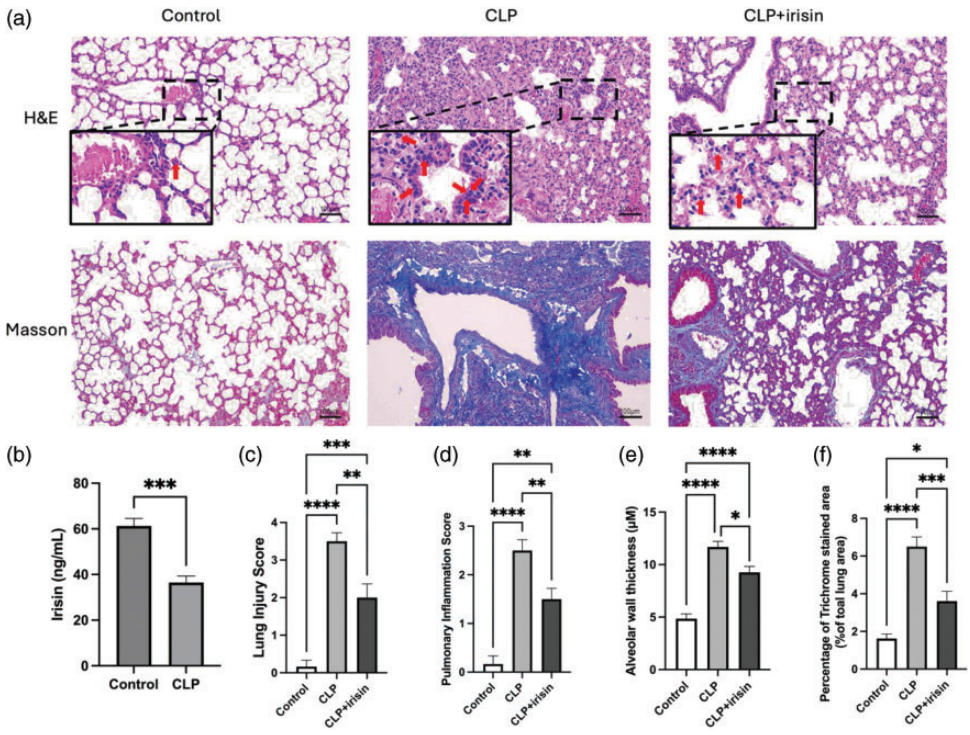

Figure 1. Irisin reduces lung injury, inflammation, and fibrosis induced by CLP. Representative images of lung tissues stained with H&E and Masson's trichrome staining from the control, CLP, and CLP + Irisin groups (a). Red arrows indicate infiltrated neutrophils within the alveolar wall. Mice were treated with Irisin for 3 days following CLP, and lung samples were collected on day 3 post-CLP. Masson staining colors indicate collagen fibers (blue), cytoplasm (pink), and nuclei (dark brown to black). Scale bar = 10 μm. Plasma irisin concentration (b), Quantitative analysis of lung injury scores (c), pulmonary inflammation scores (d), thickness of alveolar wall (e), and the percentage of lung fibrosis area (f). Statistical analysis of (b), (e), and (f) was performed using one-way ANOVA followed by Tukey's post-hoc test. Statistical analysis of histological scores (c) and (d) was performed using the Kruskal–Wallis test followed by Dunn's post-hoc test. Data are presented as means ± SEM; n = 6 per group. *$p < 0.05$; **$p < 0.01$; ***$p < 0.001$; ****$p < 0.0001$. H&E: hematoxylin and eosin; CLP: cecal ligation and puncture.

treatment significantly alleviated CLP-induced ALI.

Sepsis-induced ALI is associated with ferroptosis

To further investigate the mechanism under the ALI progression, we obtained scRNA-seq data of CLP-induced ALI model from the GEO database.[27] The standard quality control procedures were performed to remove low-quality cells, resulting in a final dataset of 29,792 lung cells. These cells included 8022 from the sham group, 11,607 from the CLP group, and 10,163 from the CLP-48h group. After clustering based on classic marker gene expression, we annotated the cells into 12 major cell types using SingleR (Figure 2(a)). Next, the ferroptosis-related gene expression profile was investigated in these cell populations. According to the heatmap and dot plot, the ferroptosis-related genes are highly expressed in CLP-induced ALI mice

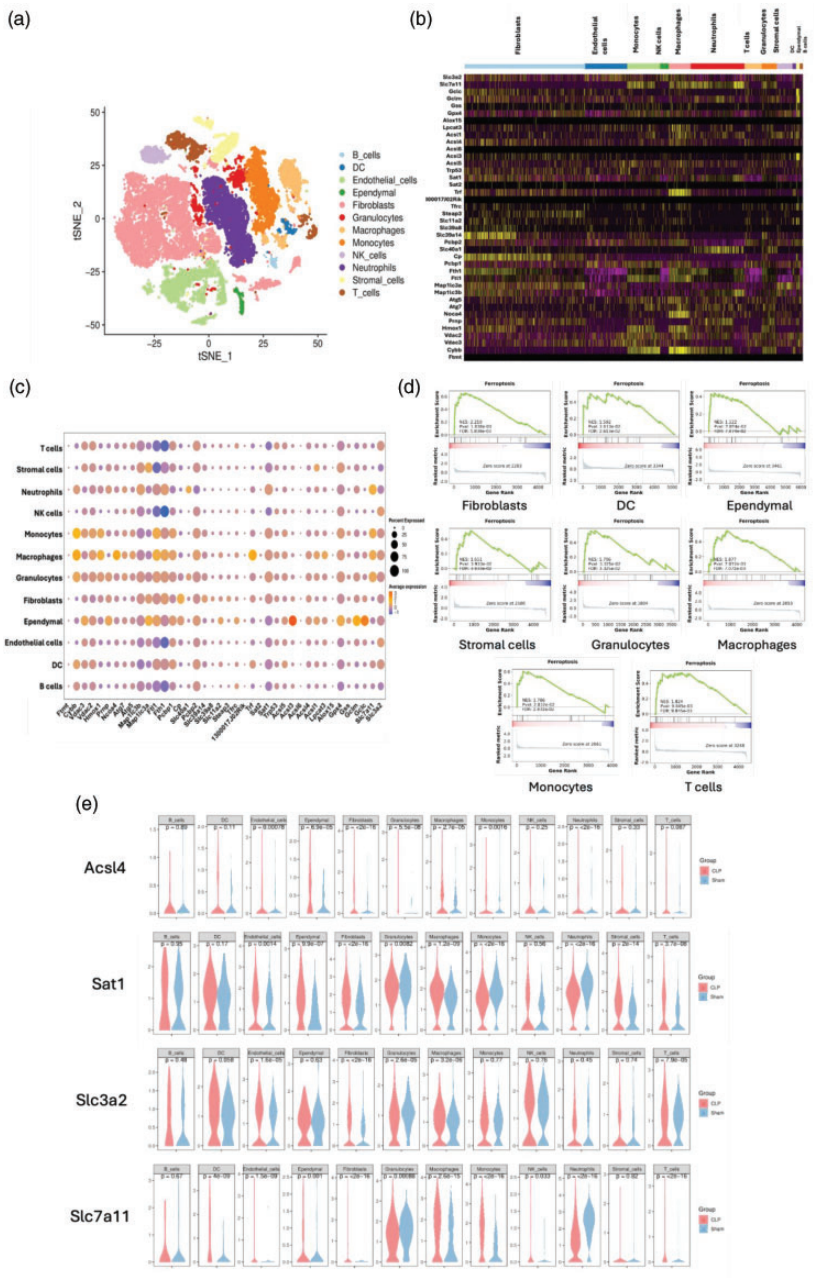

Figure 2. Single-cell transcriptomic analysis of lung cells in Sham and CLP groups. (a) t-distributed stochastic neighbor embedding plot of 29,792 lung cells from the sham and CLP groups. Cells are colored by the 12 major cell types identified based on classical marker genes. (b) Heatmap of ferroptosis-related genes. (c) Dot plot of ferroptosis-related genes. (d) Gene Set Enrichment Analysis comparing the ferroptosis gene signature between the Sham group and the combined CLP + CLP-48h group across cell types and (e) Violin plots illustrating the expression of representative ferroptosis-related genes (Slc3a2, Slc7a11, Acsl4, and Sat1), which were significantly upregulated in the CLP and CLP-48h groups compared to Sham. scRNA-seq data were obtained from the Gene Expression Omnibus database (GSE207651), and all downstream analyses were performed using the Seurat and SingleR packages in R. CLP: cecal ligation and puncture.

model (Figure 2(b) and (c)). For subsequent analysis, we combined the CLP and CLP-48 h groups to represent the ALI condition. Gene Set Enrichment Analysis revealed that the ferroptosis gene signature was upregulated in most cell types compared with the sham group (Figure 2(d)). Notably, the expression levels of Slc3a2, Slc7a11, Acsl4, and Sat1 were significantly elevated in the CLP groups, suggesting enhanced ferroptotic activity in CLP-induced lung injury (Figure 2(e)).

Irisin reduced proinflammatory cytokines in sepsis-induced ALI

The levels of proinflammatory cytokines were measured in lung tissues by ELISA. The concentrations of IL-1β (Figure 3(a)), IL-6 (Figure 3(b)), IL-18 (Figure 3(c)), and TNF-α (Figure 3(d)) were significantly higher in the CLP group compared with the control group, indicating an inflammatory response following sepsis induction. In contrast, these cytokine levels were significantly reduced in the CLP + irisin group compared with the CLP group (Figure 3 (a)–(d)), suggesting that irisin treatment mitigates CLP-induced inflammation, which is consistent with the histopathological findings.

Irisin attenuates oxidative stress during sepsis-induced ALI

As the inflammatory markers were increased in the ALI model, we further examined the ROS levels (MDA and GSH) in sepsis-induced ALI model. CLP group showed increased MDA levels and reduced GSH activity, which were reversed by irisin treatment (Figure 4(a) and (b)). Furthermore, the iron content Fe^{2+} was also examined. Fe^{2+} concentration was increased in CLP group and irisin treatment reduced the Fe^{2+} level (Figure 4(c)).

qPCR detection of ferroptosis markers in lung tissues

We further assessed the levels of ferroptosis-linked genes *Acsl4*, *Ptgs2*, and *Hspa5* to evaluate whether irisin may alleviate CLP-induced ferroptosis in the ALI

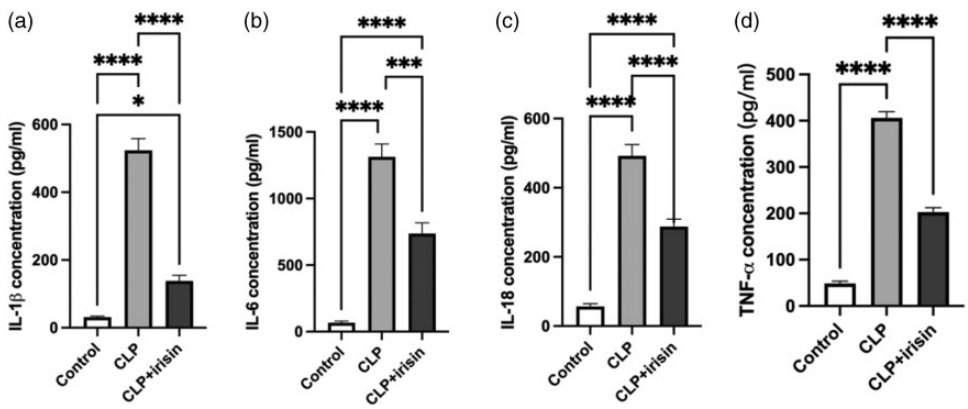

Figure 3. Enzyme-linked immunosorbent assay detection of effects of irisin on levels of inflammatory markers. (a) The levels of IL-1β in samples from lungs. (b) IL-6 level in lung samples. (c) The levels of IL-18 in the lung tissue lysate and (d) TNF-a level in lung samples. Lung tissues were harvested on day 3 post-CLP immediately after euthanasia. Statistical analysis was performed using one-way ANOVA followed by Tukey's post-hoc test. n = 6 per group. Data are presented as means ± SEM. *$p < 0.05$; ***$p < 0.001$; ****$p < 0.0001$. CLP: cecal ligation and puncture.

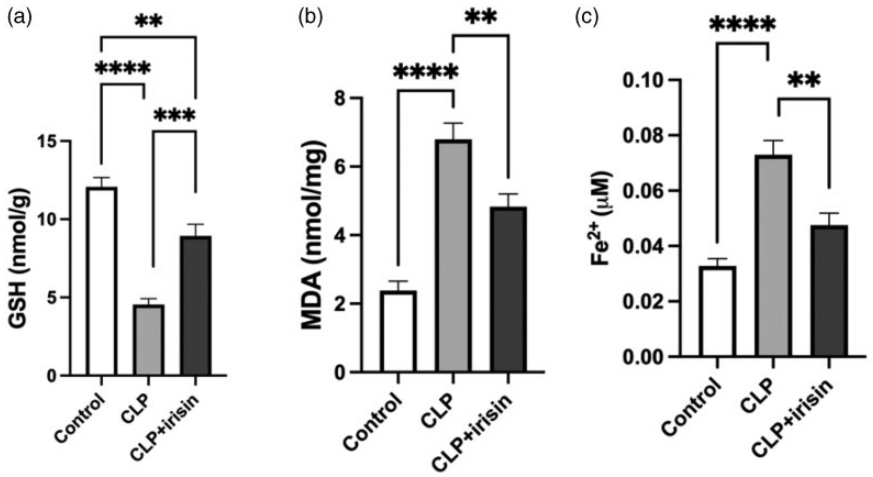

Figure 4. Irisin prevents oxidative stress following CLP damage. (a) Glutathione (GSH) concentration, (b) malondialdehyde (MDA) concentration, (c) Fe^{2+} contents in mouse lung homogenates. Lung samples were collected on day 3 post-CLP. Statistical analysis was performed using one-way ANOVA followed by Tukey's post-hoc test. n = 6 per group. Data are presented as means ± SEM. $^{**}p < 0.01$; $^{***}p < 0.001$; $^{****}p < 0.0001$. CLP: cecal ligation and puncture.

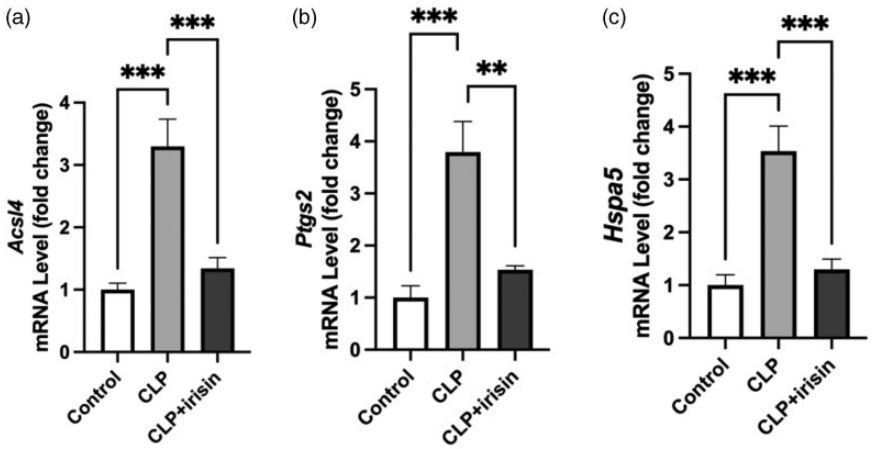

Figure 5. Quantitative polymerase chain reaction analysis on the effects of irisin on levels of *Acsl4*, *Ptgs2*, and *Hspa5* genes. Relative mRNA expression levels for the expression of (a) *Acsl4*, (b) *Ptgs2*, and (c) *Hspa5* in lung tissues. Total RNA was extracted from lung tissues harvested on day 3 post-CLP. Statistical analysis was performed using one-way ANOVA followed by Tukey's post-hoc test. n = 6 per group. Data are presented as means ± SEM. $^{**}p < 0.01$; $^{***}p < 0.001$. CLP: cecal ligation and puncture.

mice model (Figure 5). We found a significant increase in these genes in the lung samples from ALI mice compared with that in the normal lung tissues. Notably, the mRNA expression of *Acsl4*, *Ptgs2*, and *Hspa5* was significantly increased in lung tissues from ALI mice relative to the levels in control tissues (Figure 5(a)–(c)).

This indicated that CLP upregulated ferroptosis markers in the lung of mice. Specifically, relative to the CLP group, the mRNA level of *Acsl4*, *Ptgs2*, and *Hspa5* in CLP + irisin group was significantly lower. This indicated that irisin treatment alleviated the CLP-induced ALI in mice by restoring the levels of ferroptosis driving genes.

The effects of irisin on expression level of ferroptosis-related proteins

The ACSL4, COX-2, and GPX4 levels involved in the modulation of ferroptosis were further determined by western blotting. In addition, the AMP-activated protein kinase (AMPK), a well-studied protein that inhibits ferroptosis in various diseases, was also detected in this study. The levels of ACSL4 and COX-2 were elevated in CLP mice models compared with the control group, similar to the PCR results (Figure 6(a)). GPX4 is a key suppressor of ferroptosis; the GPX4 protein expression was reduced in the CLP group. However, the irisin treatment did not prevent the decrease of GPX4 (Figure 6(b)). To further investigate whether AMPK is involved in irisin treatment, we detected the downstream of AMPK phosphorylation and expression. The phosphorylation of AMPK was decreased in the CLP group, which were reversed by irisin treatment. The total AMPK (t-AMPK) was not different between the control and CLP group. Comparison between CLP and CLP + irisin group revealed that the expression of ACSL4, COX-2, and p-AMPK was significantly lower in the latter group compared with their levels in the CLP group. Nevertheless, t-AMPK levels were not significantly different between CLP and CLP + irisin group. Altogether, these results suggested that irisin may regulate ferroptosis-related proteins in ALI.

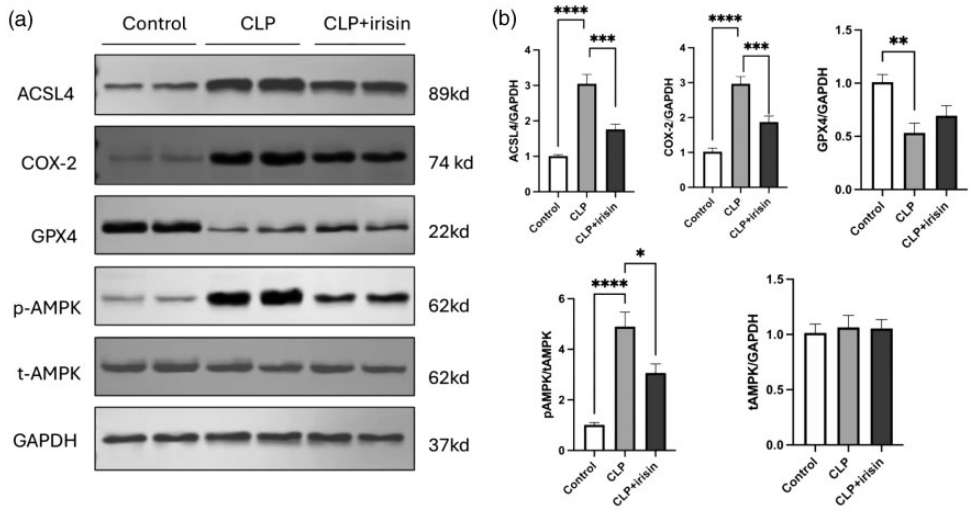

Figure 6. Western blotting analysis on the effects of irisin on the expression level of ferroptosis-associated proteins. (a) Representative western blotting images for the expression of ACSL4, COX-2, GPX4, p-AMPK, and t-AMPK in lung tissues. GAPDH was selected as the loading control protein. (b) Quantification analysis of the related bands of ACSL4, COX-2, GPX4, p-AMPK, and t-AMPK in lung tissues. Lung tissues were harvested on day 3 post-CLP. Statistical analysis was performed using one-way ANOVA followed by Tukey's post-hoc test. n = 6 per group. Data are presented as means ± SEM. *$p < 0.05$; **$p < 0.01$; ***$p < 0.001$; ****$p < 0.0001$.

Discussion

ALI is a syndrome resulting from a variety of causes that involves inflammation and enhanced pulmonary capillary permeability, leading to proteinaceous alveolar edema.[30] In our study, the histology study showed that irisin reduced the lung injury score, alveolar wall thickness, and reduced lung remodeling after CLP, which exhibited effective protection against ALI. Furthermore, irisin treatment reversed the increase of inflammatory markers in the disease model. The anti-inflammation roles of irisin have also been showed in multiple diseases.[31]

The key drivers of ALI are sepsis-associated with infections.[32] Ferroptosis promotes ALI development following infections.[33] Moreover, several inflammatory mediators also released during ALI by activation the AMPK/GSK3beta-Nrf2 signal axis.[34] The presence of inflammatory cell infiltration in the lungs during sepsis could lead to irreversible damage, ultimately culminating in ALI or even progressing to ARDS.[35] Considering that ferroptosis modulates cell death during sepsis-induced ALI, controlling this process might offer a new approach to treatment.

Irisin may inhibit ROS generation and inhibit oxidative damage in lung ischemia/reperfusion injury.[21,22] Furthermore, irisin was reported to exert antioxidant activity and suppress oxidative damage in gestational diabetes.[23] Our experiment showed that irisin reversed the GSH increasing and MDA reduction after CLP injury, which prevents oxidative stress. This study extends the anti-oxidation effect of irisin to the ALI.

Ferroptosis refers to novel type of cell death associated with iron. Typically, it manifests as accumulation of fatty acid peroxides within cells. In ALI, the concentration of free iron is significantly increased in lung tissues, disrupting iron homeostasis and leading to ferroptosis. Excessive iron in lung tissues is removed by iron chelators, deferoxamine and ciclopirox, to restore iron homeostasis and alleviate ferroptosis.[36] Moreover, GSH, a major antioxidant, influences the generation of ROS by GPX4, and is known to prevent ferroptosis.[37] This study found that sepsis-induced increased Fe^{2+} concentration and reduced GSH levels in lung tissue, which indicated that oxidation stress occurred. However, these effects were suppressed by irisin treatment. Furthermore, the GPX4 expression was also decreased in CLP group.

Several key proteins are involved in the regulation of ferroptosis, including GPX4, ACSL4, and COX-2. GPX4, an enzyme that reduces lipid hydroperoxides, is crucial for preventing ferroptosis and ACSL4 is involved in the biosynthesis of polyunsaturated fatty acids, which are substrates for lipid peroxidation. Our results from both genes and protein levels showed that irisin prevents ferroptosis after CLP injury. AMPK protein has been extensively studied that participated in ferroptosis. Previous studies showed that AMPK activation inhibited ferroptosis in cancer cells during energy stress.[38] However, a later study found that AMPK activation suppressed GPX4 expression at the transcriptional level, which promoted ferroptosis in renal cancer.[39] This suggests AMPK activation has a dual function in the regulation of ferroptosis. Interestingly, in this study, we found that irisin treatment significantly reduced ACSL4 and COX-2 expression and increased p-AMPK levels, yet it did not alter GPX4 expression. This suggests that irisin may regulate ferroptosis independently of GPX4, which is typically considered a key ferroptosis inhibitor. Previous studies indicate that AMPK activation itself could suppress ferroptosis by modulating lipid metabolism and oxidative stress, bypassing the need for GPX4 upregulation.[38] Additionally, the downregulation of

ACSL4, a crucial enzyme in lipid peroxidation, could be sufficient to mitigate ferroptosis. The suppression of COX-2, an inflammatory enzyme linked to ferroptosis progression, further supports irisin's protective effect.[40] Moreover, irisin treatment significantly reduced Fe^{2+} levels and ROS accumulation, suggesting that it may inhibit ferroptosis by reducing iron-induced oxidative stress. These findings highlight a potential GPX4-independent pathway through which irisin attenuates ferroptosis, though further mechanistic studies are required to fully elucidate its mode of action. A recent study by Han et al. found that irisin attenuates ALI by suppressing the pyroptosis of alveolar macrophages via inhibition of the HSP90/NLRP3/caspase-1/GSDMD signaling pathway.[26] Moreover, irisin has also been shown to alleviate LPS-induced ALI by suppressing miR-199a levels.[41] These findings from different groups suggest the multifunctional role of irisin in preventing ALI progression. However, before irisin could be applied clinically, more studies are needed to further elucidate its mechanisms and validate its efficacy and safety.

Although this study provides novel insights into the potential role of irisin in mitigating sepsis-induced ALI through modulation of inflammation and ferroptosis, several limitations should be acknowledged. First, the study primarily establishes associations rather than direct causation, as rescue experiments using ferroptosis inducers or inhibitors were not performed. Future studies incorporating such mechanistic approaches will be necessary to definitively confirm the role of ferroptosis in protective effects of irisin. Second, our findings are based on animal models, and further validation in human clinical samples is needed to determine the translational relevance of irisin as a potential therapeutic target for ALI. Despite these limitations, our findings contribute to the growing body of evidence supporting the potential role of irisin in reducing inflammation and ferroptosis, warranting further mechanistic and translational studies.

Conclusion

This study shows that CLP-induced ALI has increased inflammation and ferroptosis. Irisin exhibited the potential to be a treatment target by inhibiting the proinflammatory cytokines and reducing ferroptosis. Similar results were obtained in the PCR and western blot analyses for the transcription and expression levels of ferroptosis-related genes and proteins. This suggests that irisin is associated with reduced ferroptosis and inflammation in sepsis-induced ALI. These findings contribute to our understanding of the ALI pathogenesis, which offers compelling evidence for the treatment of ALI induced by sepsis. In conclusion, irisin may potentially treat ALI induced by sepsis.

Acknowledgements

None.

Author contribution

All authors have accepted responsibility for the entire content of this manuscript and consented to its submission to the journal reviewed all the results and approved the final version of the manuscript. FZ carried out experiments, analyzed and interpreted data, and wrote the manuscript. JW acquired various data. WW and GC developed the research strategy. HT designed animal works and reviewed the study. XZ conceptualized the project, designed experiments, and interpreted results.

Data availability statement

The datasets analyzed during the study are available from the corresponding author upon reasonable request.

Declaration of conflicting interests

Authors state no conflict of interest.

Ethical approval

The study was approved by the Animal Ethics Review Committee of Huai'an Fifth People's Hospital (HF209823). The research related to animal use has complied with the national regulations and institutional policies for the care and use of animals.

Funding

This research received no specific grant from any funding agency in the public, commercial, or not-for-profit sectors.

ORCID iD

Feng Zhang https://orcid.org/0009-0008-5250-2789

References

1. Fan EKY and Fan J. Regulation of alveolar macrophage death in acute lung inflammation. *Respir Res* 2018; 19: 50.
2. Zhou X and Liao Y. Gut-lung crosstalk in sepsis-induced acute lung injury. *Front Microbiol* 2021; 12: 779620.
3. Chen H, Zhang Y, Zhang W, et al. Inhibition of myeloid differentiation factor 2 by baicalein protects against acute lung injury. *Phytomedicine* 2019; 63: 152997.
4. Huppert LA, Matthay MA and Ware LB. Pathogenesis of acute respiratory distress syndrome. *Semin Respir Crit Care Med* 2019; 40: 31–39.
5. Lelubre C and Vincent JL. Mechanisms and treatment of organ failure in sepsis. *Nat Rev Nephrol* 2018; 14: 417–427.
6. Luyt C-E, Bouadma L, Morris AC, et al. Pulmonary infections complicating ARDS. *Intensive Care Med* 2020; 46: 2168–2183.
7. Fang X, Ardehali H, Min J, et al. The molecular and metabolic landscape of iron and ferroptosis in cardiovascular disease. *Nat Rev Cardiol* 2023; 20: 7–23.
8. Liu Y, Tan S, Wu Y, et al. The emerging role of ferroptosis in sepsis. *DNA Cell Biol* 2022; 41: 368–380.
9. Liu P, Feng Y, Li H, et al. Ferrostatin-1 alleviates lipopolysaccharide-induced acute lung injury via inhibiting ferroptosis. *Cell Mol Biol Lett* 2020; 25: 10.
10. Boström P, Wu J, Jedrychowski MP, et al. A PGC1-alpha-dependent myokine that drives brown-fat-like development of white fat and thermogenesis. *Nature* 2012; 481: 463–468.
11. He X, Hua Y, Li Q, et al. FNDC5/irisin facilitates muscle-adipose-bone connectivity through ubiquitination-dependent activation of runt-related transcriptional factors RUNX1/2. *J Biol Chem* 2022; 298: 101679.
12. Waseem R, Shamsi A, Mohammad T, et al. FNDC5/irisin: physiology and pathophysiology. *Molecules* 2022; 27: 1118.
13. Trettel CDS, Pelozin BRA, Barros MP, et al. Irisin: an anti-inflammatory exerkine in aging and redox-mediated comorbidities. *Front Endocrinol (Lausanne)* 2023; 14: 1106529.
14. Yin C, Hu W, Wang M, et al. Irisin as a mediator between obesity and vascular inflammation in Chinese children and adolescents. *Nutr Metab Cardiovasc Dis* 2020; 30: 320–329.
15. Zhang Y, Mu Q, Zhou Z, et al. Protective effect of irisin on atherosclerosis via suppressing oxidized low density lipoprotein induced vascular inflammation and endothelial dysfunction. *PLoS One* 2016; 11: e0158038.
16. Huangfu LX, Cai XT, Yang JN, et al. Irisin attenuates inflammation in a mouse model of ulcerative colitis by altering the intestinal microbiota. *Exp Ther Med* 2021; 22: 1433.
17. Li Q, Zhang M, Zhao Y, et al. Irisin protects against LPS-stressed cardiac damage through inhibiting inflammation, apoptosis, and pyroptosis. *Shock* 2021; 56: 1009–1018.
18. Narayanan SA, Metzger CE, Bloomfield SA, et al. Inflammation-induced lymphatic architecture and bone turnover changes are ameliorated by irisin treatment in chronic inflammatory bowel disease. *Faseb J* 2018; 32: 4848–4861.
19. Shao L, Meng D, Yang F, et al. Irisin-mediated protective effect on LPS-induced acute lung injury via suppressing inflammation and apoptosis of alveolar epithelial cells. *Biochem Biophys Res Commun* 2017; 487: 194–200.
20. Zhu W, Sahar NE, Javaid HMA, et al. Exercise-induced irisin decreases

inflammation and improves NAFLD by competitive binding with MD2. *Cells* 2021; 10: 3306.
21. Wang Y, Dong Z, Zhang Z, et al. Postconditioning with irisin attenuates lung ischemia/reperfusion injury by suppressing ferroptosis via induction of the Nrf2/HO-1 signal axis. *Oxid Med Cell Longev* 2022; 2022: 9911167.
22. Chen K, Xu Z, Liu Y, et al. Irisin protects mitochondria function during pulmonary ischemia/reperfusion injury. *Sci Transl Med* 2017; 9: eaao6298.
23. Usluogullari B, Usluogullari CA, Balkan F, et al. Role of serum levels of irisin and oxidative stress markers in pregnant women with and without gestational diabetes. *Gynecol Endocrinol* 2017; 33: 405–407.
24. Percie Du Sert N, Hurst V, Ahluwalia A, et al. The ARRIVE guidelines 2.0: updated guidelines for reporting animal research. *Br J Pharmacol* 2020; 177: 3617–3624.
25. Toscano MG, Ganea D and Gamero AM. Cecal ligation puncture procedure. *J Vis Exp* 2011; 2860.
26. Han Z, Ma J, Han Y, et al. Irisin attenuates acute lung injury by suppressing the pyroptosis of alveolar macrophages. *Int J Mol Med* 2023; 51: 32.
27. Wang F, Chen M, Ma J, et al. Integrating bulk and single-cell sequencing reveals the phenotype-associated cell subpopulations in sepsis-induced acute lung injury. *Front Immunol* 2022; 13: 981784.
28. Kadam AH, Kandasamy K, Buss T, et al. Targeting caveolae to pump bispecific antibody to TGF-beta into diseased lungs enables ultra-low dose therapeutic efficacy. *PLoS One* 2022; 17: e0276462.
29. Curtis JL, Warnock ML, Arraj SM, et al. Histologic analysis of an immune response in the lung parenchyma of mice. Angiopathy accompanies inflammatory cell influx. *Am J Pathol* 1990; 137: 689–699.
30. Zhu W, Zhang Y and Wang Y. Immunotherapy strategies and prospects for acute lung injury: focus on immune cells and cytokines. *Front Pharmacol* 2022; 13: 1103309.
31. Slate-Romano JJ, Yano N and Zhao TC. Irisin reduces inflammatory signaling pathways in inflammation-mediated metabolic syndrome. *Mol Cell Endocrinol* 2022; 552: 111676.
32. Fowler AA 3rd, Truwit JD, Hite RD, et al. Effect of vitamin C infusion on organ failure and biomarkers of inflammation and vascular injury in patients with sepsis and severe acute respiratory failure: the CITRIS-ALI randomized clinical trial. *JAMA* 2019; 322: 1261–1270.
33. Yin X, Zhu G, Wang Q, et al. Ferroptosis, a new insight into acute lung injury. *Front Pharmacol* 2021; 12: 709538.
34. Lv H, Liu Q, Wen Z, et al. Xanthohumol ameliorates lipopolysaccharide (LPS)-induced acute lung injury via induction of AMPK/GSK3beta-Nrf2 signal axis. *Redox Biol* 2017; 12: 311–324.
35. Kumar V and Chhibber S. Acute lung inflammation in Klebsiella pneumoniae B5055-induced pneumonia and sepsis in BALB/c mice: a comparative study. *Inflammation* 2011; 34: 452–462.
36. Liu X, Zhang J and Xie W. The role of ferroptosis in acute lung injury. *Mol Cell Biochem* 2022; 477: 1453–1461.
37. Dixon SJ, Lemberg KM, Lamprecht MR, et al. Ferroptosis: an iron-dependent form of nonapoptotic cell death. *Cell* 2012; 149: 1060–1072.
38. Lee H, Zandkarimi F, Zhang Y, et al. Energy-stress-mediated AMPK activation inhibits ferroptosis. *Nat Cell Biol* 2020; 22: 225–234.
39. Li Y, Zhang Y, Qiu Q, et al. Energy-stress-mediated AMPK activation promotes GPX4-dependent ferroptosis through the JAK2/STAT3/P53 axis in renal cancer. *Oxid Med Cell Longev* 2022; 2022: 2353115.
40. Deng L, He S, Guo N, et al. Molecular mechanisms of ferroptosis and relevance to inflammation. *Inflamm Res* 2023; 72: 281–299.
41. Ma LY, Liu JM, Du GL, et al. Irisin attenuates lipopolysaccharide-induced acute lung injury by downregulating inflammatory cytokine expression through miR-199a-mediated Rad23b overexpression. *Exp Cell Res* 2021; 404: 112593.